# A Green Chemistry Approach for the Synthesis of Flower-like Ag-Doped MnO2 Nanostructures Probed by Surface-Enhanced Raman Spectroscopy

**ARTICLE** *in* THE JOURNAL OF PHYSICAL CHEMISTRY C · JANUARY 2009

Impact Factor: 4.77 · DOI: 10.1021/jp809561p



**8 AUTHORS**, INCLUDING:

Surojit Pande
Birla Institute of Technology and Science P…
**45** PUBLICATIONS **1,629** CITATIONS
SEE PROFILE

Arun Kumar
Center for Environmental Planning and Te…
**256** PUBLICATIONS **3,169** CITATIONS
SEE PROFILE

Sandip Saha
National Sun Yat-sen University
**21** PUBLICATIONS **492** CITATIONS
SEE PROFILE

Tarasankar Pal
IIT Kharagpur
**254** PUBLICATIONS **8,743** CITATIONS
SEE PROFILE

THE JOURNAL OF PHYSICAL CHEMISTRY C



Article

# A Green Chemistry Approach for the Synthesis of Flower-like Ag-Doped MnO Nanostructures Probed by Surface-Enhanced Raman Spectroscopy

Subhra Jana, Surojit Pande, Arun Kumar Sinha, Sougata Sarkar, Mukul Pradhan, Mrinmoyee Basu, Sandip Saha, and Tarasankar Pal

*J. Phys. Chem. C*, **2009**, 113 (4), 1386-1392• DOI: 10.1021/jp809561p • Publication Date (Web): 02 January 2009

# A Green Chemistry Approach for the Synthesis of Flower-like Ag-Doped $MnO_2$ Nanostructures Probed by Surface-Enhanced Raman Spectroscopy

**Subhra Jana, Surojit Pande, Arun Kumar Sinha, Sougata Sarkar, Mukul Pradhan, Mrinmoyee Basu, Sandip Saha, and Tarasankar Pal***

*Department of Chemistry, Indian Institute of Technology, Kharagpur 721 302, India*

*Received: October 29, 2008; Revised Manuscript Received: November 12, 2008*

Novel hierarchical flower-like nanostructures of Ag-doped $MnO_2$ have been obtained by facile wet chemical and photochemical routes. UV−visible absorption spectroscopy measurement reveals that doping of Ag nanoparticles in $MnO_2$ nanostructures leads to a red shift of the absorption edge and reduces the optical band gap energy from 2.68 to 2.51 eV while compared with undoped $MnO_2$. Raman study reveals that the band broadens and shifts toward higher wavenumbers as the $MnO_6$ octahedron is contorted by Ag doping and thus the loss of translational symmetry activates otherwise Raman-forbidden oxygen vibrations. Finally, SERS activity upsurges from Ag-doped $MnO_2$ with Rhodamine 6G and 2-aminothiophenol as probe molecules.

## 1. Introduction

Over the past few years, the controlled synthesis of inorganic micro- and nanostructures with well-defined shapes and sizes has attracted increasing interest because of their widespread potential applications, including photonics, nanoelectronics, catalysis, information storage, biosensors, and spectroscopy.[1−3] Recently, much effort has been directed to fabricate nanomaterials with different shapes, such as nanobelts, nanowires, nanotubes, nanocubes, nanoboxes, hollow spheres, etc.[4−6] The simplest synthetic route to obtain these novel architectures is probably self-assembly, in which ordered aggregates are formed in a spontaneous process.[7] As a recently developed concept, the self-assembly technique is proved to be an efficient "bottom-up" synthetic route in fabricating functional materials with different patterns and morphologies.[8,9] So far, two strategies have been developed through bottom-up synthetic route for nanostructured materials: the first one is the use of hard templates, which physically confine the size and shape of the growing nanoparticles,[10,11] and the second is use of capping agents/surfactants during nanoparticle growth to control its dimension, direction, and morphology.[12] Using these simple synthetic routes, many complicated hierarchical nanostructures, including inorganic[13,14] and organic nanostructures,[15,16] have been fabricated. These hierarchical structures are expected to play an important role in producing the next generation microelectronic and optoelectronic devices because they can be used as both building units and interconnects.[17,18] However, it is still a challenge to develop simple and facile synthetic route for hierarchically self-assembled architectures with designed chemical components and controlled morphologies, which will strongly affect the properties of nanomaterials.

Semiconductor nanoparticles or quantum dots possess size-dependent optical absorption and photoluminescence (PL) response.[19,20] These properties arise from confining charge carriers (quantum confinement) to semiconductor physical dimensions that approach the Bohr radius of an electrostatically bound electron−hole pair or exciton in the bulk material.[21,22] Being a smart and environmentally friendly semiconductor, $MnO_2$ has attracted much attention because of its physical and chemical properties and wide range of applications in catalysis, ion exchange, molecular adsorption, biosensors, and particularly, energy storage.[23,24] $MnO_2$ exists in many polymorphic forms (such as $\alpha$, $\beta$, $\gamma$, and $\delta$) because the basic unit $MnO_6$ octahedral is linked in different ways.[25,26] Apart from nanoparticles, different one-dimensional (1D) $MnO_2$ nanostructures such as rods, wires, tubes, etc. have been fabricated using hydrothermal techniques.[27,28] However, integration of 1D nanostructure building blocks into two- and three-dimensional (2D and 3D) ordered nanostructured semiconducting materials is still considerably more difficult and is highly desirable for advanced nanoscale electronic and optoelectronic applications.[29,30] Thus, it remains a great challenge to develop a facile method for solution phase synthesis of 3D hierarchical nanostructures of $MnO_2$ at room temperature. Moreover, low-temperature synthesis in aqueous solutions always represents an environmentally benign and user-friendly approach, which may be considered to be a green chemical alternative of practical significance.[31,32]

An effective method for manipulating the physical properties of semiconductors involves impurity doping.[33] Doped nanomaterials provide the possibility for enhanced, multimodal functionality in contrast to their single-component counterparts.[34] Selective doping with various metal ions using ion impregnation and chemical doping procedure has proven to be an efficient route to improve the photoactivity and enhance the photocatalytic activity of doped semiconductor nanoarchitectures.[35,36] Furthermore, the size of nanoparticles as well as the mode of deposition of metal nanoparticles plays a crucial role while tailoring the properties of semiconductor nanomaterials.[37] Recently, silver-doped $V_2O_5$ was shown to significantly improve the intercalation rate, specific capacity, and cycling performance in lithium ion batteries.[38] Kamat et al. reported that the photoelectrochemical performance of nanostructured $TiO_2$ films can be improved by coupling them with noble metal nanoparticles.[39−41] They illustrated photoinduced charge distribution and Fermi-level equilibration events in ZnO−metal nanocomposite particles and so on. But there is no report of the synthesis of Ag-doped $MnO_2$ nanoarchitecture to inherit enhanced electromagnetic effect for enlightening SERS activity.

Herein, we report for the first time a green chemistry approach for the synthesis of flower-like Ag-doped $MnO_2$ 3D nanoarchi-

* Corresponding author. E-mail: tpal@chem.iitkgp.ernet.in.

10.1021/jp809561p CCC: $40.75 
Published on Web 01/02/2009

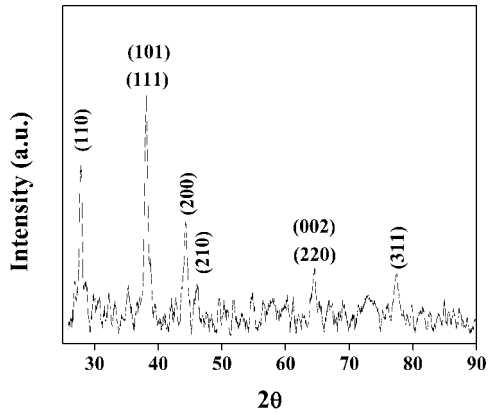


**Figure 1.** XRD pattern of Ag-doped $MnO_2$ nanostructures.

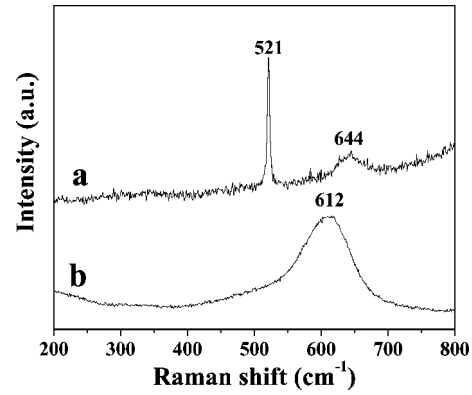


**Figure 2.** Raman spectra of (a) $MnO_2$ nanorod and (b) Ag-doped $MnO_2$ nanostructures.

tecture at room temperature. The solution phase synthetic procedure involved wet chemical oxidation of Mn(II) precursor followed by reduction of doped Ag(I) ion. The reduction was performed separately through chemical and photochemical means which generate flower-like nanostructures. The highly stable nanostructured materials have been characterized by different physical methods. UV−visible absorption spectroscopy has been exploited to estimate the band gap energy. Raman study shows that the band broadens and shifts toward higher wavenumbers as the $MnO_6$ octahedron is contorted by Ag doping and thus the loss of translational symmetry activates otherwise Raman-forbidden oxygen vibrations. Finally, we have studied the SERS activity of Ag-doped $MnO_2$ nanoflowers exploiting 2-aminothiophenol (2-ATP) and Rhodamine 6G (R6G) as probe molecules.

## 2. Experimental Methods

**2.1. Synthesis of Rod-Shaped $MnO_2$ Nanoparticles.** According to our previously reported method[42] we have synthesized $MnO_2$ rod-shaped particles. An aqueous solution containing manganese(II) chloride ($MnCl_2 \cdot 4H_2O$, $5 \times 10^{-3}$ M) and sodium dodecylbenzenesulfonate (SDBS, $5 \times 10^{-2}$ M) was stirred with a magnetic stirrer at room temperature. Under this stirring condition, aqueous NaOH solution was introduced to the reaction mixture drop by drop to obtain its final concentration of $5 \times 10^{-3}$ M and the stirring was continued for 15 min. The colorless reaction mixture turned initially to light brown and finally to dark brown which indicates the onset of the evolution of the $MnO_2$ nanoparticles. Now, the brown solution was kept overnight.

**2.2. Synthesis of Ag-Doped $MnO_2$ Nanoflowers.** Ag-doped $MnO_2$ nanoflower was synthesized as follows: an aqueous solution of $AgNO_3$ (400 $\mu$L, 10 mM) was added to the above synthesized brown-colored solution containing rod-shaped $MnO_2$ nanoparticles (8 mL, 5 mM) and then the mixture was stirred with a magnetic stirrer for 24 h. After that, the solution was centrifuged at 10 000 rpm for 10 min. The supernatant was discarded to remove the free $MnO_2$, and the residue was collected and redispersed in water. The residue was washed 10 times with distilled water. Then the residue was dispersed in 4 mL of water and divided into two parts. In one portion, aqueous solution of $NaBH_4$ (200 $\mu$L, 0.1 mM) was added and stirred gently for 5 min. The other solution was irradiated under 60 W tungsten bulb for 2 days under stirring condition. The light brown solution was characterized by different physical methods keeping the solution for 24 h. Scheme 1 depicts the formation of nanoflowers.

**2.3. Synthesis of R6G/Ag-$MnO_2$ and ATP/Ag-$MnO_2$ Assemblies.** For SERS study we have taken wet chemically synthesized Ag-doped $MnO_2$ nanoflowers as a substrate. A stock solution of ATP (10 mM) was prepared in ethanol. Then, the 20 $\mu$L of $10^{-4}$ M ethanolic solution of ATP was added to the different sets of solution containing Ag-doped $MnO_2$ nanoflowers so that the final concentration of ATP becomes $10^{-5}$, $10^{-6}$, and $10^{-7}$ M. Similarly, 20 $\mu$L of $10^{-4}$ M dye solution (R6G) was added to the different sets of nanoflower solutions so that the final concentration of dye in the experiment became $10^{-5}$, $10^{-6}$, and $10^{-7}$ M, and the resulting solutions were incubated for 12 h before the SERS studies.

**SCHEME 1: Schematic Presentation of Nanoflower Formation**

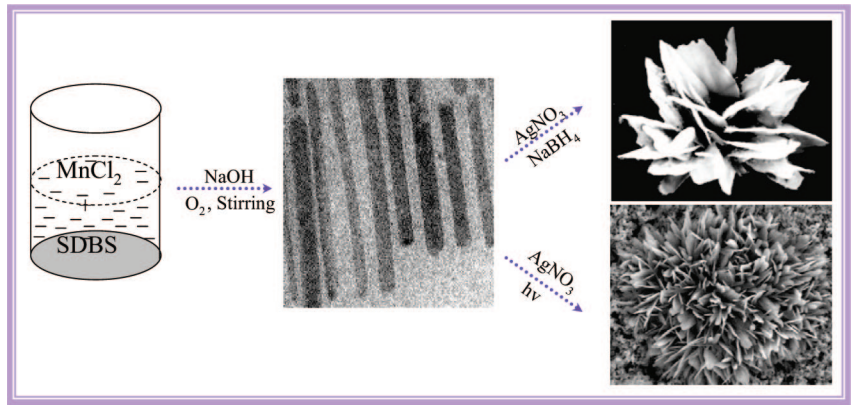

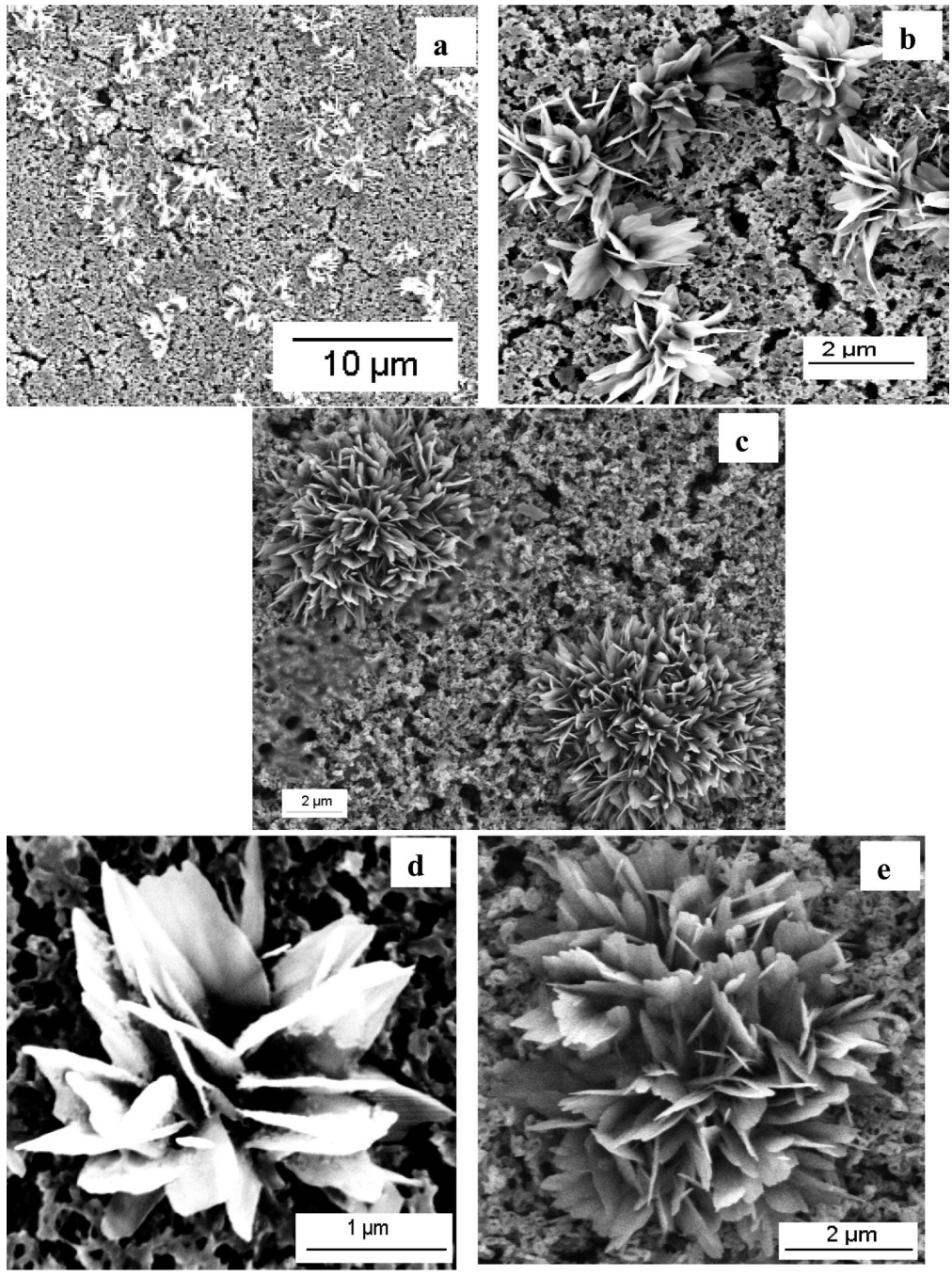


**Figure 3.** FE-SEM images of flower-like nanoarchitectures (a, b, and d) synthesized by wet chemical and (c and e) photochemical routes.

## 3. Results and Discussion

**3.1. Characterization of the Particles.** The phase and purity of the products are examined by X-ray diffraction (XRD) on PW3040/60 X-ray diffractometer with Cu Kα radiation ($\lambda$ =1.54178 Å), the operation voltage and current maintained at 40 kV and 30 mA respectively. The representative XRD pattern of the wet chemically synthesized product is illustrated in Figure 1. All the diffraction peaks of the product can be indexed to be Ag doped $\beta$-$MnO_2$. The XRD peaks can be well assigned to the planes (110), (101), (210), and (002) for $MnO_2$ and (111), (200), (220), and (311) for Ag, respectively. From this figure, it is observed that the peaks shift from their standard positions in the presence of the dopant. The shift in the lattice parameter is mainly due to the dopant occupying interstitial positions in the lattice.[43,44] No indication of silver oxide impurities in the final product is observed. The relatively broader diffraction peaks suggest the smaller crystallite size of the Ag-doped $MnO_2$ nanoarchitecture.

In our previous report, we demonstrated that Raman spectrum of $\beta$-$MnO_2$ nanorods[42] consists of two well-defined sharp peaks appear at 521 and 644 $cm^{-1}$ and the three weak bands at 209, 344, and 440 $cm^{-1}$. It is worth mentioning that, in $MnO_2$, Raman absorption comes from the collective vibration mode of $MnO_6$ octahedron. The two main Raman peaks correspond to the stretching mode of the $MnO_6$ octahedra and the peaks at lower wavenumber are attributed to the deformation modes of the metal−oxygen chain of Mn−O−Mn in the $MnO_2$ octahedral lattice. Upon doping of Ag in $MnO_2$, the band broadens and shifts toward higher wavenumbers (Figure 2). It is reported that the $MnO_6$ octahedron is contorted by metal doping and the loss of translational symmetry activates otherwise Raman-forbidden oxygen vibrations, corresponding to the off-center phonon

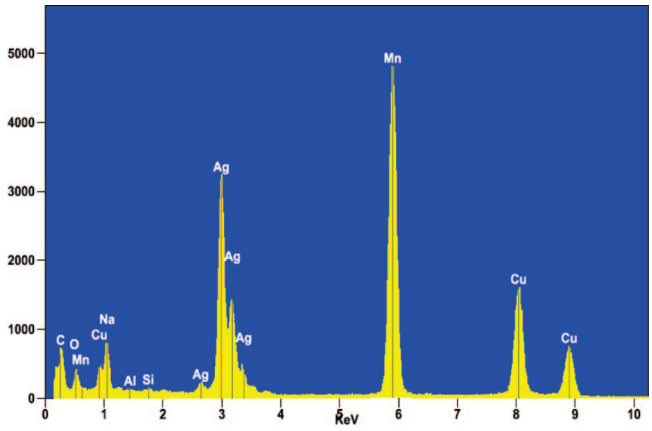


**Figure 4.** EDX spectrum of Ag-doped $MnO_2$ nanoflowers synthesized by wet chemical route.

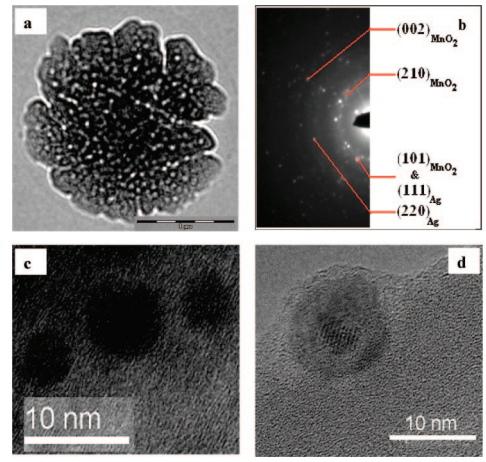


**Figure 5.** (a) TEM image of a single nanoflower, (b) corresponding SAED pattern, and (c, d) doped Ag nanoparticles on the nanoflower.

modes in the ordered parent compound. As a consequence of the loss of translational symmetry and the activation of otherwise forbidden vibrations, the relatively broad bands in the Raman spectra for high substitution levels reflect the phonon density of states rather than the Raman-allowed zone center phonons.[45,46]

The morphology of the synthesized product was characterized by field-emission scanning electron microscopy (FE-SEM). Figure 3 demonstrates the FE-SEM images of the synthesized products by wet chemical (a, b, and d) as well as photochemical (c and e) routes. An overall view in Figure 3a indicates many flower-like nanoarchitectures. A closer examination reveals that the flower-like nanostructures are aligned in various directions from a common central zone (Figure 3, b and c). The high-magnification image in Figure 3d shows that a single flowery nanostructure is made of tiny nanopetals growing outside from different sites of a main trunk which are 1.25 $\mu$m in length and 500 nm in diameter. It should be worth mentioning that this nanostructure cannot be destroyed into discrete petals even under long-time sonication, indicating that the nanoflowers are actually integrated strongly and are not delicate aggregates.

The composition of the synthesized product was further confirmed from EDX analysis. The EDX pattern of the nanoflowers is presented in the Figure 4. The EDX analysis confirms both wet chemically and photochemically synthesized products composed of Mn, O, and Ag. The amount of silver in different nanopetals is very consistent. We observed a homogeneous distribution of dopant, i.e., Ag, in the final product and no sign of a lateral or longitudinal concentration gradient in individual petals. This is due to the Ag(I) ion impregnation in $MnO_2$ matrix by ion-exchange mechanism.

The TEM image of a wet chemically synthesized nanoflower is presented in Figure 5a. The nanopetals are 1.25 $\mu$m in length and 500 nm in diameter. Figure 5b represents the SAED pattern of the nanoflower indicating polycrystalline nature and the bright spots are due to the (210), (101), and (002) planes for $MnO_2$ and (111) and (220) planes for Ag. The dopant Ag particles have an average diameter of 8 $\pm$ 2 nm, shown in Figure 5, c and d.

**3.2. Growth Mechanism.** It is known that SDBS is an ionic compound which ionizes completely in water. During nanomaterial synthesis, SDBS serves as a "soft" template and/or a capping agent. So far, SDBS has been systematically studied in the synthesis of nanostructured materials and may form spherical, cylindrical micelles depending on the solution concentrations.[47,48] We have already reported that above the critical micellar concentration (cmc), SDBS forms rodlike micellar template and that rodlike micellar template contributes to the rod formation and subsequently stabilizes the particles. Now, we have discovered that deliberate incorporation of Ag(I) ion in turn Ag(0) changes the morphology of $MnO_2$ nanoparticles bringing in Raman activity and then quality SERS from the flowery architectures.

In 1D oriented nanorods, electric dipole is the driving force[49,50] and this would be the case in O═Mn═O. But in the case of 3D oriented nanoflowers, neither the electric dipole nor the magnetic dipole plays a deterministic role. The growth mechanism of the synthesized nanoflower might be similar as reported earlier.[51] The nanopetals consist of many tiny nanorods. These nanorods were constructing blocks for the formation of the nanoflowers. In aqueous solution $MnO_2$ behaves as a cation exchanger.[52] Hence homogeneous distribution of Ag(I) ion onto the nanorods is understandable. After the adsorption of Ag(I) ions, the tiny nanorods are precipitated. The discarded supernatant solution is mainly with $MnO_2$ nanorods devoid of Ag(I) ion. This is verified experimentally. Then Ag(I)-bound nanorods of $MnO_2$ are reduced to produce Ag-doped $MnO_2$ nanostructures by wet chemical or photochemical route. Such tiny nanorods aligned to form a bundle of independent nanorods which coalesced and fused together to form a single petal, driven by the reduced interfacial energy.[53,54] However, the fact is that the nucleation and growth of the nanorod from a main trunk demands less nucleating energy. Moreover, after the incorporation of silver ion in SDBS-stabilized $MnO_2$ nanorods, repetitive washing decreased the surfactant concentration in the reaction medium. Thus, lower surfactant concentration provides a prospect to coalesce Ag bearing many nanorods which in turn support nanoflower formation. Again, during the growth of nanocrystals, formation of 3D nanoarchitectures should always be thermodynamically favorable because of the reduced surface free energy of the individual crystals. Interestingly, larger nanoflower is produced by photochemical procedure because of the slower reduction rate compared to wet chemical method. However, the self-assembly procedure of the Ag doped nanorod to form a nanoflower is yet to be understood and needs further investigation.

**3.3. Optical Property.** The optical property of the nanoflowers is investigated by UV−visible absorption spectroscopy. UV−visible absorption spectrum of $MnO_2$ nanorod shows a broad peak in the region of 300−400 nm, centered at ~309 nm. The optical band gap $E_g$ for the semiconductor has been graphically determined from the equation $\alpha E_p = K(E_p - E_g)^{1/2}$

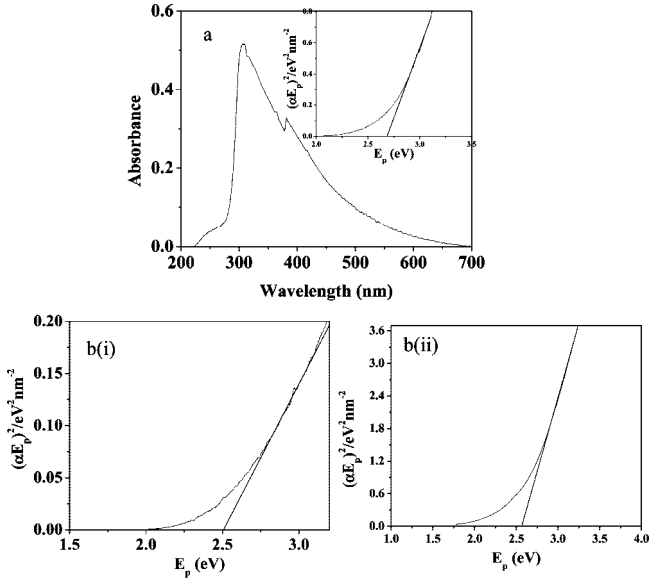


**Figure 6.** UV−visible absorption spectra and the corresponding $(\alpha E_p)^2$ vs $E_p$ curves for (a) $MnO_2$ nanorod and (b) Ag-doped $MnO_2$ nanoflowers synthesized by (i) wet chemical and (ii) photochemical routes.

(where α is the absorption coefficient, $K$ is a constant, $E_p$ is the discrete photo energy, and $E_g$ is the band gap energy);[55] a classical Tauc approach is further employed to estimate the $E_g$ value of the nanoflowers. The plot of $(\alpha E_p)^2$ versus $E_p$ based on the direct transition for $MnO_2$ nanorod is presented in Figure 6a. The band gap energy for $MnO_2$ nanorod is derived as 2.68 eV from the extrapolated value (the straight lines to the $X$ axis) of $E_p$ at $\alpha = 0$. The optical absorption of the $MnO_2$ nanorods in the visible light range originates mainly from d−d transitions of Mn ions. Mn 3d energy level splits into higher ($e_g$) and lower ($t_{2g}$) energy levels due to the ligand field of $MnO_6$ octahedra. The band gap energy corresponds to the energy difference between Mn 3d $t_{2g}$ and $e_g$ states. Mn 3d $t_{2g}$ and $e_g$ states serve as the "valence band" and the "conduction band" of the semiconductor, respectively.[56] The increase in the band gap energy for the $MnO_2$ nanorods compared to bulk $MnO_2$ is indicative of quantum confinement effects. It is already reported that Introduction of metal ion can tune the band gap of metal oxide.[57,58] The UV−visible spectra for Ag-doped $MnO_2$ nanoflowers show that incorporation of Ag into $MnO_2$ leads to a red shift in the optical response and a concomitant reduction of the band gap energy (Figure 6b). The optical band gap $E_g$ of the nanoflowers obtained by wet chemical and photochemical routes is estimated to be 2.51 and 2.56 eV, respectively.

**3.4. Application in SERS.** Since its discovery,[59] surface-enhanced Raman scattering (SERS) has played an important role in studies of molecules adsorbed onto metal surfaces. The discovery of SERS cannot only increase the sensitivity of Raman spectroscopic detection but also helps to reveal the orientation of the molecules and the mechanism about the interaction of the molecules with the substrate. Very excitingly, the nanoparticle arrays exhibit size-tunable surface-enhanced Raman scattering, an analytical technique which can integrate high chemical sensitivity with spectroscopic precision and has enormous potential for trace chemical detection.[60,61] Recent progress in surface-enhanced Raman spectroscopy has made single molecule detection possible, which is of considerable interest to the researchers concerned with nanomaterials, analytical chemistry, and single molecule spectroscopy.[62−64] The most widely used metals with the appropriate optical characteristics in the visible to near-IR are Ag and Au, although other metals can also support

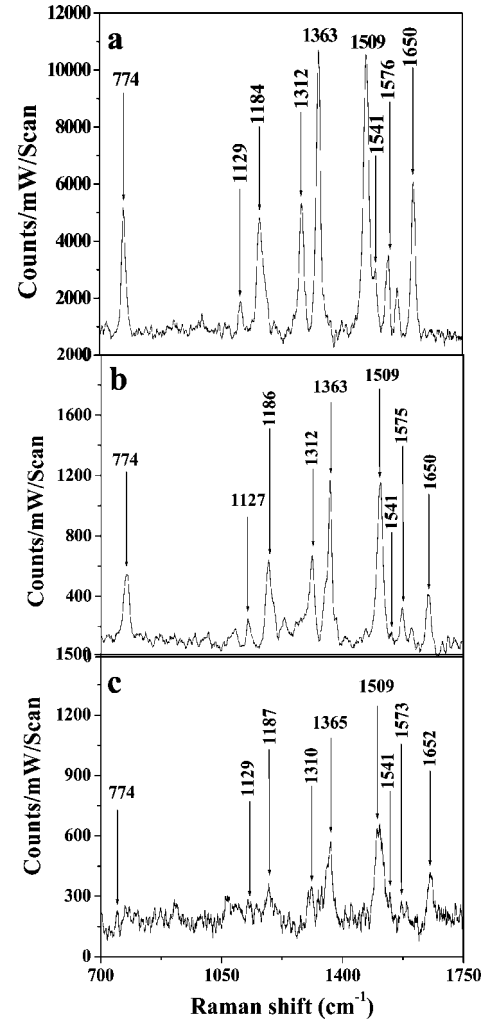


**Figure 7.** SERS spectra of R6G (a, $10^{-5}$ M; b, $10^{-6}$ M; and c, $10^{-7}$ M) for Ag-doped $MnO_2$ nanoflowers.

SERS activity at different wavelengths of laser light. Under these conditions, enhancement of the Raman signal of $10^6$ can be obtained. SERS enhancements of $10^{12}-10^{14}$ have been reported by many researchers at the junctions between the closely spaced nanoparticles, which has opened up a new avenue of using Raman techniques for single molecule detection.[62−64] The SERS enhancement mechanism originates in part from the large local electromagnetic fields caused by resonant surface plasmons that can be optically excited at certain wavelengths for metal particles of different shapes or closely spaced groups of particles.[65−67] In addition to electromagnetic field enhancement, metal nanostructures and molecules can form charge-transfer complexes that provide further enhancement for SERS.[68,69]

The SERS activity of Ag-doped $MnO_2$ nanoflowers was examined using R6G and 2-ATP as probe molecules. Here, doped Ag nanoparticles on the $MnO_2$ matrix contribute to the SERS enhancement. R6G is a strongly fluorescent xanthene derivative which shows a molecular resonance Raman (RR) effect when excited into its visible absorption band. Figure 7 show a set of SERS spectra of R6G molecules adsorbed on Ag-doped $MnO_2$ nanoflowers at different concentrations. R6G is chemisorbed to the active site via an Ag−N bond. The observed Raman bands that are assigned to R6G include $\nu$(C−H) out-of-plane bending mode at 774 $cm^{-1}$, $\nu$(C−H) in-plane bending mode at 1129 $cm^{-1}$, and $\nu$(C−C) stretching modes at 1363, 1509, and 1650 $cm^{-1}$.[70]

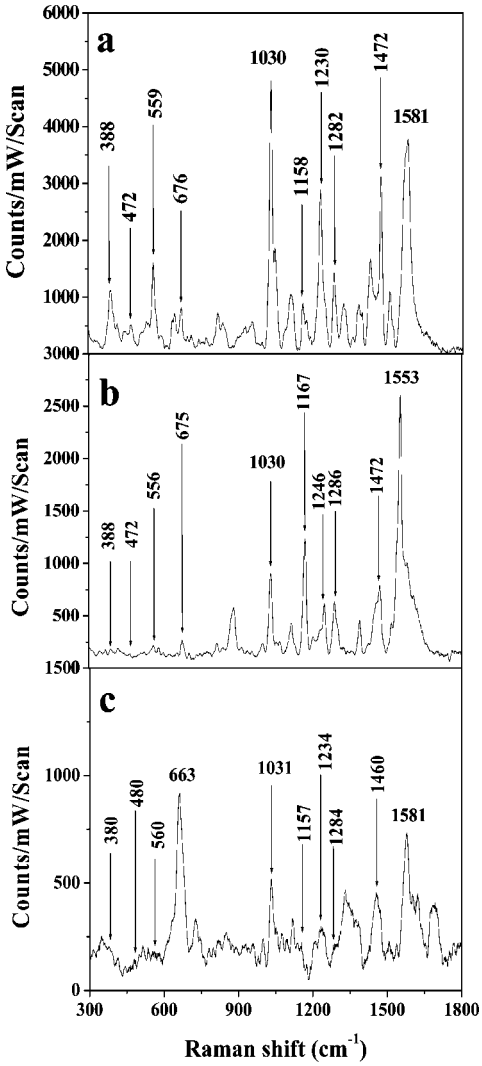


**Figure 8.** SERS spectra of 2-ATP (a, $10^{-5}$ M; b, $10^{-6}$ M; and c, $10^{-7}$ M) for Ag-doped $MnO_2$ nanoflowers.

Figure 8 depicts another set of SERS spectra of 2-ATP at different concentrations adsorbed on nanoflower surfaces. 2-ATP molecules are adsorbed onto the Ag surfaces via their "N" and "S" atoms[71,72] as the in-plane vibrations $\nu$(C−N), $\nu$(C−S) stretching mode and $\delta$(C−S) bending mode at 1309, 484, and 370 $cm^{-1}$ have been shifted to 1282, 472, and 388 $cm^{-1}$, respectively, and weakly enhanced after 2-ATP adsorption to the Ag surface. The lower degree of enhancement is observed for $\delta$(C−C) and $\delta$(C−H) bending modes at 676 and 1158 $cm^{-1}$, respectively. The higher degree of enhancement is observed for in-plane vibrations such as $\nu$(C−C) at 1567 and 1472 $cm^{-1}$ and $\delta$(C−H) at 1030 $cm^{-1}$, respectively. There are also some in-plane bending modes such as $\delta$(C−C) at 559 $cm^{-1}$ and $\delta$(C−H) at 1230 $cm^{-1}$, which have also been strongly enhanced.

It was already established that the SERS enhancement is the result of a combination of electromagnetic effect and chemical effect. But chemical effect is generally thought to contribute only a factor of $10-10^2$, compared to $10^4-10^7$ for electromagnetic effect.[71−74] In the present study, the SERS enhancement of the samples is expected to arise from both electromagnetic effect and chemical effect. As there is no need to add any extra aggregating agent from outside, we can conclude that the electromagnetic field enhancement plays the major role. Ag nanoparticles doped on nanoflowers would excite localized surface plasmon resonance (LSPR) under laser irradiation,

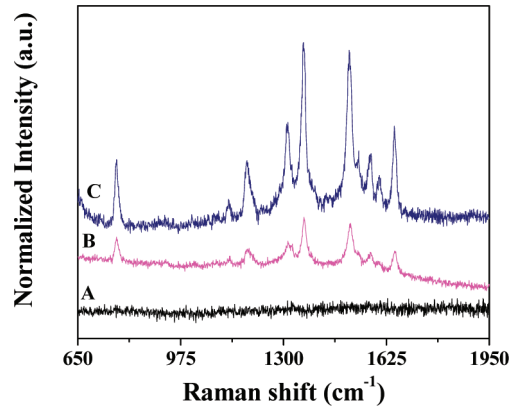


**Figure 9.** SERS spectra of $1 \times 10^{-5}$ M R6G with (A) $MnO_2$, (B) Ag hydrosol, and (C) Ag-doped $MnO_2$ nanoflowers.

**TABLE 1: Apparent Enhancement Factor (AEF) for Different Concentrations of (A) 2-ATP Molecules and (B) R6G Molecules Adsorbed on Ag-Doped $MnO_2$ Nanoflowers**

| (A) 2-ATP Molecules | |
|---|---|
| concn of ATP | AEF at 1030 $cm^{-1}$ |
| $10^{-5}$ | $2.16 \times 10^5$ |
| $10^{-6}$ | $4.05 \times 10^5$ |
| $10^{-7}$ | $2.23 \times 10^6$ |
| **(B) R6G Molecules** | |
| concn of R6G | AEF at 1363 $cm^{-1}$ |
| $10^{-5}$ | $1.06 \times 10^3$ |
| $10^{-6}$ | $6.10 \times 10^3$ |
| $10^{-7}$ | $3.70 \times 10^4$ |

enhancing the SERS signals of the probe molecules through long-range electromagnetic enhancement. Moreover, the apparent enhancement factor (AEF) has been calculated using the following equation:

$$\mathrm{AEF} = \sigma_{\mathrm{SERS}}[C_{\mathrm{NRS}}]/\sigma_{\mathrm{NRS}}[C_{\mathrm{SERS}}]$$

where $C_{NRS}$ is the concentration of the molecules in the bulk samples, $C_{SERS}$ is the concentration of the adsorbed molecules on the silver surface, and $\sigma_{NRS}$ and $\sigma_{SERS}$ are the intensities of a certain vibration in normal Raman spectra and SERS spectra, respectively. The enhancement factor has been calculated for R6G and 2-ATP adsorbed on Ag-doped $MnO_2$ nanoflowers surfaces and presented in Table 1. It may be mentioned that, nanoflowers synthesized both by photochemical as well as wet chemical routes exhibit comparable SERS signal enhancement with R6G and 2-ATP molecules and these probe molecules do not exhibit any SERS activity from undoped $MnO_2$ substrate. It is worth noting that even under the same experimental condition R6G shows weak SERS while examined with standard silver hydrosol.[75] A comparative account of all the above-mentioned substrates for SERS activity with R6G has been represented in Figure 9.

## 4. Conclusions

In conclusion, hierarchical flower-like Ag-doped $MnO_2$ nanostructures have been achieved by a facile wet chemical as well as photochemical routes. Incorporation of Ag into $MnO_2$ leads to a red shift in the optical response and a concomitant reduction of the band gap energy from 2.68 to 2.51 eV. Finally, SERS activity of the nanoflowers has been investigated suc-

cessfully using R6G and ATP as probe molecules, which is not possible with undoped $MnO_2$. Because of the green chemistry approach, cost, simplicity and reproducibility, the synthesis reported here can be readily scaled up.

**Acknowledgment.** We are thankful to the Council of Scientific and Industrial Research (CSIR), the University Grants Commission (UGC), the Department of Science and Technology (DST), New Delhi, and Indian Institute of Technology, Kharagpur, for financial assistance. This work is dedicated to Prof. J. A. Creighton for his pioneering work in surface enhanced Raman spectroscopy.

## References and Notes

(1) Puntes, V. F.; Krishnan, K. M.; Alivisatos, A. P. *Science* **2001**, *291*, 2115.
(2) Jin, R.; Cao, Y. W.; Mirkin, C. A.; Kelly, K. L.; Schatz, G. C.; Zheng, J. G. *Science* **2001**, *294*, 1901.
(3) Murphy, C. J.; Jana, N. R. *Adv. Mater.* **2002**, *14*, 80.
(4) Morales, A. M.; Lieber, C. M. *Science* **1998**, *279*, 208.
(5) Pan, Z. W.; Dai, Z. R.; Wang, Z. L. *Science* **2001**, *291*, 1947.
(6) Sun, Y. G.; Xia, Y. N. *Science* **2002**, *298*, 2176.
(7) Whitesides, G. M.; Boncheva, M. *Proc. Natl. Acad. Sci. U.S.A.* **2002**, *99*, 4937.
(8) Corma, A.; Rey, F.; Rius, J.; Sabater, M. J.; Valencia, S. *Nature* **2004**, *431*, 287.
(9) Lu, W. G.; Gao, P. X.; Jian, W. B.; Wang, Z. L.; Fang, J. Y. *J. Am. Chem. Soc.* **2004**, *126*, 14816.
(10) Foss, C. A.; Hornyak, G. L.; Stockert, J. A.; Martin, C. R. *J. Phys. Chem.* **1994**, *98*, 2963.
(11) Nicewarner-Pena, S. R.; Freeman, G. P.; Reiss, B. D.; He, L.; Pena, D. J.; Walton, I. D.; Cromer, R.; Keating, C. D.; Natan, M. J. *Science* **2001**, *294*, 137.
(12) Jana, N. R.; Gearheart, L. A.; Murphy, C. J. *J. Phys. Chem. B* **2001**, *105*, 4065.
(13) Ni, X. M.; Zhao, Q. B.; Zhang, D. E.; Zhang, X. J.; Zheng, H. G. *J. Phys. Chem. C* **2007**, *111*, 601.
(14) Narayanaswamy, A.; Xu, H. F.; Pradhan, N.; Kim, M.; Peng, X. G. *J. Am. Chem. Soc.* **2006**, *128*, 10310.
(15) Breen, T. L.; Tien, J.; Oliver, S. R. J.; Hadzic, T.; Whitesides, G. M. *Science* **1999**, *284*, 948.
(16) Cao, A. M.; Hu, J. S.; Liang, H. P.; Wan, L. J. *Angew. Chem., Int. Ed.* **2005**, *44*, 4391.
(17) Fan, H. J.; Werner, P.; Zacharias, M. *Small* **2006**, *6*, 700.
(18) Ding, Y. S.; Shen, X. F.; Gomez, S.; Luo, H.; Aindow, M.; Suib, S. L. *Adv. Funct. Mater.* **2006**, *16*, 549.
(19) Brus, L. E. *Appl. Phys. A: Mater. Sci. Process.* **1991**, *53*, 465.
(20) Alivisatos, A. P. *Science* **1996**, *271*, 933.
(21) Wang, Y.; Herron, N. *J. Phys. Chem.* **1991**, *95*, 525.
(22) Weller, H. *Angew. Chem., Int. Ed. Engl.* **1993**, *32*, 41.
(23) Li, Z.; Ding, Y.; Xiong, Y.; Xie, Y. *Cryst. Growth Des.* **2005**, *5*, 1953.
(24) Subramanian, V.; Zhu, H.; Vajtai, R.; Ajayan, P. M.; Wei, B. *J. Phys.Chem. B* **2005**, *109*, 20207.
(25) Cheng, F.; Zhao, J.; Song, W.; Li, C.; Ma, H.; Chen, J.; Shen, P. *Inorg. Chem.* **2006**, *45*, 2038.
(26) Wang, X.; Li, Y. *J. Am. Chem. Soc.* **2002**, *124*, 2880.
(27) Wang, X.; Li, Y. D. *Chem. Eur. J.* **2003**, *9*, 300.
(28) Yuan, Z. Y.; Ren, T. Z.; Du, G. H.; Su, B. L. *Appl. Phys. A: Mater. Sci. Process.* **2005**, *80*, 743.
(29) Ng, H. T.; Li, J.; Smith, M. K.; Nguyen, P.; Cassell, A.; Han, J.; Meyyappan, M. *Science* **2003**, *300*, 1249.
(30) (a) Jiang, J. C.; Henry, L. L.; Gnanasekar, K. I.; Chen, C. L.; Meletis, E. I. *Nano Lett.* **2004**, *4*, 741. (b) Yuan, J.; Laubernds, K.; Zhang, Q.; Suib, S. L. *J. Am. Chem. Soc.* **2003**, *125*, 4966.
(31) Peng, X. *Chem. Eur. J.* **2002**, *8*, 334.
(32) Zhao, N. N.; Qi, L. M. *Adv. Mater.* **2006**, *18*, 359.
(33) Shi, W.; Zeng, H.; Sahoo, Y.; Ohulchanskyy, T. Y.; Ding, Y.; Wang, Z. L.; Swihart, M.; Prasad, P. N. *Nano Lett.* **2006**, *6*, 875.
(34) Wang, S.; Jarrett, B. R.; Kauzlarich, S. M.; Louie, A. Y. *J. Am. Chem. Soc.* **2007**, *129*, 3848.
(35) Nakato, Y.; Shioji, M.; Tsubomura, H. *Chem. Phys. Lett.* **1982**, *90*, 453.
(36) Kamat, P. V. *J. Phys. Chem. B* **2002**, *106*, 7729.
(37) Hiesgen, R.; Meissner, D. *J. Phys. Chem. B* **1998**, *102*, 6549.
(38) Hosono, E.; Fujihara, S.; Imai, H.; Honma, I.; Masaki, I.; Zhou, H. *ACS Nano* **2007**, *1*, 273.
(39) Subramanian, V.; Wolf, E.; Kamat, P. V. *J. Phys. Chem. B* **2001**, *105*, 11439.
(40) Hirakawa, T.; Kamat, P. V. *Langmuir* **2004**, *20*, 5645.
(41) Subramanian, V. E.; Wolf, E.; Kamat, P. V. *J. Phys. Chem. B* **2003**, *107*, 7479.
(42) Jana, S.; Basu, S.; Pande, S.; Ghosh, S. K.; Pal, T. *J. Phys. Chem. C* **2007**, *111*, 16272.
(43) Brahma, R.; Krishna, M. G.; Bhatnagar, A. K. *Bull. Mater. Sci.* **2006**, *29*, 317.
(44) Yuhas, B. D.; Zitoun, D. O.; Pauzauskie, P. J.; He, R.; Yang, P. *Angew. Chem., Int. Ed.* **2006**, *45*, 420.
(45) Lorenz, M. B.; Litvinchuk, A. P.; Wang, Y. Q.; Sun, Y. Y.; Chu, C. W. *J. Phys.: Condens. Matter* **2005**, *17*, 3333.
(46) Hu, L.; Tong, W.; Zhu, H.; Zhang, Y. *J. Phys.: Condens. Matter* **2003**, *15*, 2033.
(47) Qiao, Z. -P.; Zhang, Y.; Zhou, L.-T.; Xire, Q. *Cryst. Growth Des.* **2007**, *7*, 2394.
(48) Jia, X.; Chen, D.; Jiao, X.; He, T.; Wang, H.; Jiang, W. *J. Phys. Chem. C* **2008**, *112*, 911.
(49) Cho, K.-S.; Talapin, D. V.; Gaschler, W.; Murray, C. B. *J. Am. Chem. Soc.* **2005**, *127*, 7140.
(50) Yu, J. H.; Joo, J.; Park, H. M.; Baik, S. I.; Kim, Y. W.; Kim, S. C.; Hyeon, T. *J. Am. Chem. Soc.* **2005**, *127*, 5662.
(51) Wu, J. M.; Qi, B. *J. Phys. Chem. C* **2007**, *111*, 666.
(52) Greenwood, N. N.; Earnshaw, A. *Chemistry of the Elements*, 1st ed.; Pergamon Press Ltd.: New York, 1984; p 1219.
(53) Penn, R. L.; Banfield, J. F. *Science* **1998**, *281*, 969.
(54) Li, Q. C.; Kumar, V.; Li, Y.; Zhang, H. T.; Marks, T. J.; Chang, R. P. H. *Chem. Mater.* **2005**, *17*, 1001.
(55) Tsunekawa, S.; Fukuda, T.; Kasuya, A. *J. Appl. Phys.* **2000**, *87*, 1318.
(56) Sakai, N.; Ebina, Y.; Takada, K.; Sasaki, T. *J. Phys. Chem. B* **2005**, *109*, 9651.
(57) Dietl, T.; Ohno, H.; Matsukura, F.; Gilbert, J.; Ferrand, D. *Science* **2000**, *287*, 1019.
(58) Park, J. H.; Kim, S.; Bard, A. J. *Nano Lett.* **2006**, *6*, 24.
(59) Fleischman, M.; Hendra, P. J.; McQuillan, A. J. *Chem. Phys. Lett.* **1974**, *26*, 163.
(60) Albrecht, M. G.; Crieghton, J. A. *J. Am. Chem. Soc.* **1977**, *99*, 5215.
(61) Kneipp, K.; Kneipp, H.; Itzkan, I.; Dasari, R. R.; Feld, M. S. *Chem. Rev.* **1999**, *99*, 2957.
(62) Nie, S. M.; Emory, S. R. *Science* **1997**, *275*, 1102.
(63) Xu, H.; Bjerneld, E. J.; Kä ll, M.; Bö rjesson, L. *Phys. Rev. Lett.* **1999**, *83*, 4357.
(64) Futamata, M. *Faraday Discuss.* **2006**, *132*, 45.
(65) Moskovits, M. *J. Chem. Phys.* **1978**, *69*, 4159.
(66) Yang, W. H.; Schatz, G. C.; Van Duyne, R. P. *J. Chem. Phys.* **1995**, *103*, 869.
(67) Xu, H.; Azipurua, J.; Kall, M.; Apell, P. *Phys. Rev. E* **2000**, *62*, 4318.
(68) Jiang, J.; Busnick, K.; Maillard, M.; Brus, L. *J. Phys. Chem. B* **2003**, *107*, 9964.
(69) Otto, A. *J. Raman Spectrosc.* **2005**, *36*, 497.
(70) Hildebrandt, P.; Stockburger, M. *J. Phys. Chem.* **1984**, *88*, 5935.
(71) Liz-Marzan, L. M.; Giersig, M.; Mulvaney, P. *Langmuir* **1996**, *12*, 4329.
(72) Nikoobakht, B.; EI-Sayed, M. A. *J. Phys. Chem. A* **2003**, *107*, 3372.
(73) Zhang, J.; Li, X.; Sun, X.; Li, Y. *J. Phys. Chem. B* **2005**, *109*, 12544.
(74) Doering, W.; Nie, S. *J. Phys. Chem. B* **2002**, *106*, 311.
(75) Creighton, J. A.; Blatchford, C. G.; Albrecht, M. G. *J. Chem. Soc., Faraday Trans.* **1979**, *75*, 790.

JP809561P